

Narrowline Laser Cooling and Spectroscopy of Molecules via Stark States

Kameron Mehling,¹ Justin J. Burau,¹ Logan E. Hillberry,¹ Mengjie Chen,¹ Parul Aggarwal,¹ Lan Cheng,² Jun Ye,¹ and Simon Scheidegger¹

¹*JILA, National Institute of Standards and Technology and the University of Colorado, Boulder, Colorado 80309-0440
Department of Physics, University of Colorado, Boulder, Colorado 80309-0390, USA*

²*Department of Chemistry, The Johns Hopkins University, Baltimore, Maryland 21218, USA
(Dated: March 19, 2025)*

The electronic energy level structure of yttrium monoxide (YO) provides long-lived excited $^2\Delta$ states ideal for high-precision molecular spectroscopy, narrowline laser cooling at the single photon-recoil limit, and studying dipolar physics with unprecedented interaction strength. We use ultracold laser-cooled YO molecules to study the Stark effect in the metastable $A'^2\Delta_{3/2} J = 3/2$ state by high-resolution laser spectroscopy. We determined the absolute transition frequency from this metastable state to the $X^2\Sigma^+$ electronic ground state with a fractional uncertainty of 9×10^{-12} . In the presence of weak electric fields a linear Stark effect is observed in the $A'^2\Delta_{3/2}$ state owing to the large electric dipole moment and near degenerate Λ -doublet states. A quasi-closed photon cycling scheme is identified involving a narrowline transition to a single Stark state, and implemented in free space to demonstrate the first narrowline laser cooling of a molecule, reducing the temperature of sub-Doppler cooled YO in two dimensions.

I. INTRODUCTION

Polar molecules are versatile quantum systems with a broad range of applications in the fields of precision spectroscopy [1], searches for fundamental symmetry violations [2–4], quantum simulation of strongly interacting systems [5–10], quantum computation [11–15], and cold chemistry [16, 17]. The rich internal structure of polar molecules is appealing for these applications; the exploitable features include narrow transitions over a broad spectral range, close lying states of opposite parity, and strong intermolecular interactions. This complexity of the molecular structure makes it challenging to control the external and internal degrees of freedom. In pioneering work, many experimental techniques have been developed to control the motion using inhomogeneous electric and magnetic fields [18–21], and internal states by optical pumping [22, 23]. Today, the direct laser cooling of molecules provides a route towards combined control on the single quanta level.

The primary challenge for molecular laser cooling has been identifying photon cycling schemes. Early proposals suggested that vibrational closure is accessible in molecules with highly diagonal Franck-Condon factors [24]. In addition, rotational closure is established by utilizing a P(1) transition between a rotationally excited $X^2\Sigma^+$ ground state and a non-rotating $^2\Pi$ or $^2\Sigma^+$ excited state [25]. Following this recipe, direct laser cooling of diatomic and polyatomic molecules has been achieved [26–28], along with confinement in magneto-optical traps [29–33], sub-Doppler cooling [34–39], and optical dipole trapping with densities high enough to study two-body collisions [40] at the single partial wave limit [41]. Whereas all these successes utilized strong P(1) transitions, the use of other excited electronic states can further expand the quantum state control available to molecules.

Most laser cooled diatomic molecules possess a $^2\Delta$

state in the vicinity of the energetically lowest $^2\Pi$ state. If the $^2\Delta$ is the first excited electronic state (below the $^2\Pi$), rotational closure is weakly broken, as a two-photon decay pathway to an opposite-parity ground state becomes accessible [42]. However, this electronic state configuration yields metastable $^2\Delta$ states with many unique features to utilize: *i*) The long natural lifetime of the excited state allows for precise optical molecular spectroscopy; *ii*) The narrow transition linewidth enables laser cooling to the photon recoil limit [43–45]; *iii*) The near degenerate Λ -doublet states and the large electric dipole moment ($\mu_e \approx 7$ D) facilitate dc electric-field collisional shielding and strong dipolar interactions at electric field strengths orders of magnitude lower than currently proposed [46–49].

With this strong motivation, we present quantum state control of the $^2\Delta$ state within a laser-cooled molecule. Our techniques are demonstrated with yttrium monoxide ($^{89}\text{Y}^{16}\text{O}$) and extend to a class of other metal-monoxide molecules. The manuscript is structured as follows: In Sec. II we introduce the low-lying electronic energy level structure of metal monoxides $M^{16}\text{O}$ ($M = ^{45}\text{Sc}, ^{89}\text{Y}, ^{139}\text{La}, ^{227}\text{Ac}$), focusing on the properties of the $^2\Delta$ state. Section III introduces the experimental techniques used for preparing ultracold YO molecules. Section IV presents our results on high-resolution optical spectroscopy of $A'^2\Delta \leftarrow X^2\Sigma^+$ transitions. Section V presents the first narrowline laser cooling of a molecule (see Refs. [43–45] for proposals). Finally, Sec. VI presents conclusions drawn from this YO case study.

II. ENERGY LEVEL STRUCTURE

The common energy level structure of MO molecules arises from the strong ionic bond involving a single va-

lence electron localized at the metal center. Figure 1 schematically depicts the ordering of the lowest excited electronic states of metal monoxides $M^{16}\text{O}$. They all have the same $\Sigma-\Delta-\Pi$ electronic state ordering, providing a metastable ${}^2\Delta$ state [50–54] with a natural lifetime much longer than the ${}^2\Pi$ state. The lowest electronic states have been well characterized and the spectroscopic constants for ScO, YO and LaO are available with sufficient accuracy for the broad transitions [50–58]. However, only a few studies of the long-lived ${}^2\Delta$ states are available [53, 59] and important properties such as the Λ -doublet splitting remain unresolved.

The angular momentum coupling in the $X\,{}^2\Sigma^+$ ground state is dominated by the interaction between electron-spin and nuclear-spin and best described using a Hund's case ($b_{\beta S}$) coupling scheme. The large Fermi contact interaction leads to two energetically well-separated manifolds with a total spin $\mathbf{G} = \mathbf{I} + \mathbf{S}$, where \mathbf{S} is the total electron spin and \mathbf{I} is the nuclear spin of the metal nucleus. The rotational angular momentum \mathbf{N} couples with \mathbf{G} to form the total angular momentum including spins $\mathbf{F} = \mathbf{N} + \mathbf{G}$. The notation (N, G, F) will be used to specify the quantum numbers of the $X\,{}^2\Sigma^+$ state. This electronic state possesses definite parity, alternating between positive and negative parity according to $(-1)^N$ for a given rotational manifold.

The angular momentum coupling in the $A'\,{}^2\Delta$ and $A\,{}^2\Pi$ excited electronic states is dominated by the spin-orbit interaction and best described by a Hund's case (a) coupling scheme. The term symbol ${}^{2S+1}|\Lambda||\Sigma|$ describes the electronic state, $2S+1$ is the spin multiplicity, Λ and Σ are the projections of the electronic orbital angular momentum and electron spin onto the internuclear axis, and $\Omega = \Lambda + \Sigma$. The letters $\Sigma, \Pi, \Delta, \dots$ are used to represent $|\Lambda| = 0, 1, 2, \dots$ in the term symbol. Since the projection of the angular momentum onto the internuclear axis can be positive or negative, there exist two quantum states (Λ doublet) with identical magnitudes of Σ , Λ , and Ω . The parity eigenfunctions for the Hund's case (a) basis are

$$|\eta, \Lambda, \Sigma, \Omega, \pm\rangle = \frac{1}{\sqrt{2}} (|\eta, \Lambda, \Sigma, \Omega\rangle \pm |\eta, -\Lambda, -\Sigma, -\Omega\rangle), \quad (1)$$

where η contains all other quantum numbers, such as the vibrational quantum number v , the total angular momentum quantum number J , the total angular momentum quantum number including spin F , and the projection quantum number m_F required to define each quantum state [60, 61].

The energy degeneracy of the ${}^2\Pi$ Λ doublets is lifted by interactions with nearby ${}^2\Sigma^+$ states. Since each rotational state in ${}^2\Sigma^+$ states has a fixed parity, a parity-dependent perturbation is induced through spin-orbit (SO) and electronic-rotational interactions [62–64]. The perturbations result in a Λ -doublet splitting that strongly depends on the underlying coupling strength and the energy difference $\Delta E = |E_{\Pi} - E_{\Sigma}|$ between the electronic energy states. In the lowest rotational states of the $A\,{}^2\Pi$

electronic state, the Λ -doublet splitting can be estimated by the Mulliken parameter $q \approx 4B^2/\Delta E$ for ${}^2\Pi_{3/2}$ [63], where B is the rotational constant. Homogeneous SO interactions ($\Delta\Omega = 0$) are usually $A_{\text{SO}}^{\Pi}/B \approx 10^3$ times stronger than heterogeneous electronic-rotational interactions ($\Delta\Omega = \pm 1$), where A_{SO}^{Π} is the spectroscopically resolved spin-orbit coupling constant of the ${}^2\Pi$ state. Thus, the Λ -doublet splitting for the ${}^2\Pi_{1/2}$ state can be estimated as $p \approx qA_{\text{SO}}^{\Pi}/B$ [63]. The same mechanisms apply to the Λ -doublet splitting of ${}^2\Delta$ states via perturbation from the lifted degeneracy of the parity doublets within the nearby ${}^2\Pi$ states [65].

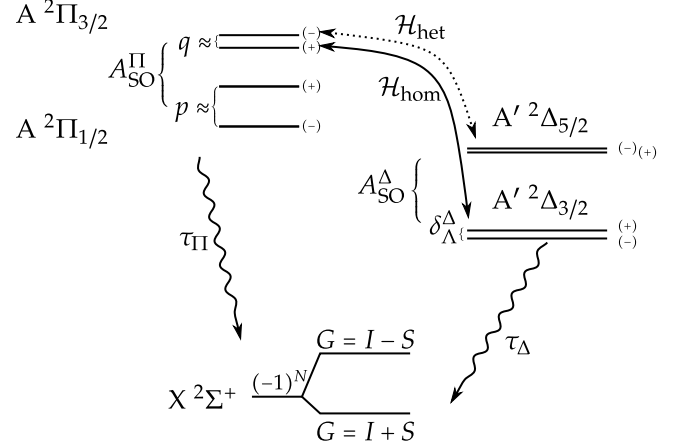


FIG. 1: Energy level diagram of the lowest three electronic states in the diatomic MO molecules. The large Fermi contact interaction dominates the fine structure in the $X\,{}^2\Sigma^+$ ground electronic state, whereas, the spin-orbit interaction (A_{SO}) is dominant in the ${}^2\Pi$ and ${}^2\Delta$ excited states. The lifetime and the Λ -doublet splitting in the ${}^2\Delta$ state are primarily inherited from the ${}^2\Pi_{3/2}$ state through homogeneous \mathcal{H}_{hom} and heterogeneous \mathcal{H}_{het} interactions depicted by the double arrows. The parity of each state is depicted within the parentheses.

The radiative lifetime (τ) and the Λ -doublet splitting of the $A'\,{}^2\Delta_{3/2}$ state are dominated by the admixed $A\,{}^2\Pi_{3/2}$ character resulting from the homogeneous interaction \mathcal{H}_{hom} . This class of metal monoxide molecules possess effective off-diagonal spin-orbit coupling matrix elements much smaller than the spectroscopic resolved spin-orbit coupling constant [54], leading to lifetimes $\tau_{\Delta} \sim (10\,\mu\text{s})$, about 10^3 of the ${}^2\Pi$ state lifetime τ_{Π} . The admixture of the $A\,{}^2\Pi_{3/2}$ state determines not only the lifetime, but also the Λ -doubling splitting $\delta_{\Lambda}^{\Delta} \approx q\tau_{\Pi}/\tau_{\Delta} \sim q \cdot 10^{-3}$ ($\delta_{\Lambda}^{\Delta} \approx 6\,\text{kHz}$ for YO). The ${}^2\Delta_{5/2}$ state admixing with ${}^2\Pi_{3/2}$ is even further suppressed as it results from the heterogeneous interaction \mathcal{H}_{het} . Therefore, the radiative decay rate and the Λ -doublet splitting of the ${}^2\Delta_{5/2}$ state are expected to be at least 10^3 smaller than in the ${}^2\Delta_{3/2}$ state. The dominant interactions for each

electronic state and relative energy splittings are shown diagrammatically in Fig. 1.

The near degeneracy of the opposite-parity Λ -doublet states and the large internal electric dipole moment of several Debye (7.8 D for YO [66]) makes the ${}^2\Delta$ states extraordinarily sensitive to external electric fields. The Stark interaction can be calculated precisely for the lowest J states, where rotational distortion is negligible. The field dependent energy levels can be obtained by diagonalizing the effective Hamiltonian

$$\mathcal{H}_{\text{tot}} = \mathcal{H}_0 + \mathcal{H}_S, \quad (2)$$

where \mathcal{H}_0 contains the field free energy levels and \mathcal{H}_S represents the non-relativistic Stark effect. The Stark effect matrix elements using parity symmetrized eigenfunctions are calculated following Ref. [60]

$$\begin{aligned} \langle \Omega, J, I, F, m_F, \pm | T_0^1(\mu_e) T_0^1(\mathbf{E}) | \Omega, J', I, F', m_F, \mp \rangle = \\ -\mu_e E (-1)^{F-F'-m_F+I-\Omega} \Theta(F) \Theta(F') \Theta(J) \Theta(J') \\ \begin{pmatrix} F & 1 & F' \\ -m_F & 0 & m_F \end{pmatrix} \begin{Bmatrix} J' & F' & I \\ F & J & 1 \end{Bmatrix} \begin{pmatrix} J & 1 & J' \\ -\Omega & 0 & \Omega \end{pmatrix}, \end{aligned} \quad (3)$$

where μ_e is the electric dipole moment of the ${}^2\Delta_{3/2}$ state, E is the electric field strength, and $\Theta(x) = \sqrt{2x+1}$. Since the hyperfine splitting is much larger than δ_Λ^Δ one can restrict the calculation in the weak field limit to a single value of Ω , J and F . This simplifies the matrix elements in Eq. (3) to

$$\begin{aligned} \langle \Omega, J, I, F, m_F, \pm | T_0^1(\mu_e) T_0^1(\mathbf{E}) | \Omega, J, I, F, m_F, \mp \rangle = \\ -\mu_e \frac{J(J+1) + F(F+1) - I(I+1)}{2F(F+1)J(J+1)} |\Omega| E m_F := \\ -\mu_{\text{eff}} E m_F. \end{aligned} \quad (4)$$

The Stark interaction induced by electric fields on the order of $10^{-3} \text{ V cm}^{-1}$ is comparable to δ_Λ^Δ and polarizes the molecule in the laboratory frame. The field dependent $|m_F| \neq 0$ states are aligned to the electric field and no longer possess definite parity. This implies that the parity selection rule for dipole transitions involving these states is no longer valid [see Fig. 2 (b)].

The spontaneous decay $A'{}^2\Delta \rightarrow X^2\Sigma^+$ paths do not obey rotational closure, but one can limit the branching to two rotational manifolds in the ground electronic state. The decay pathways for YO are depicted in Fig. 2 (b), where we use $[J, F, |m_F|^P]$ to specify all relevant quantum numbers of the ${}^2\Delta_{3/2}$ state and if necessary an additional parity label $p \in \{+, -, \div\}$ for a positive, negative, or mixed parity state, respectively. The branching ratios from $A'{}^2\Delta_{3/2}[3/2, 1, |m_F|^P]$ to the ground electronic state are calculated using the Hund's case (b) to (a) basis transformation provided in Ref. [67]. The spontaneous decay to even rotational states is equally distributed between $N = 0$ and $N = 2$. Conversely, the decay to odd rotational states possess 90% branching to the $N = 1$ manifold. This branching provides

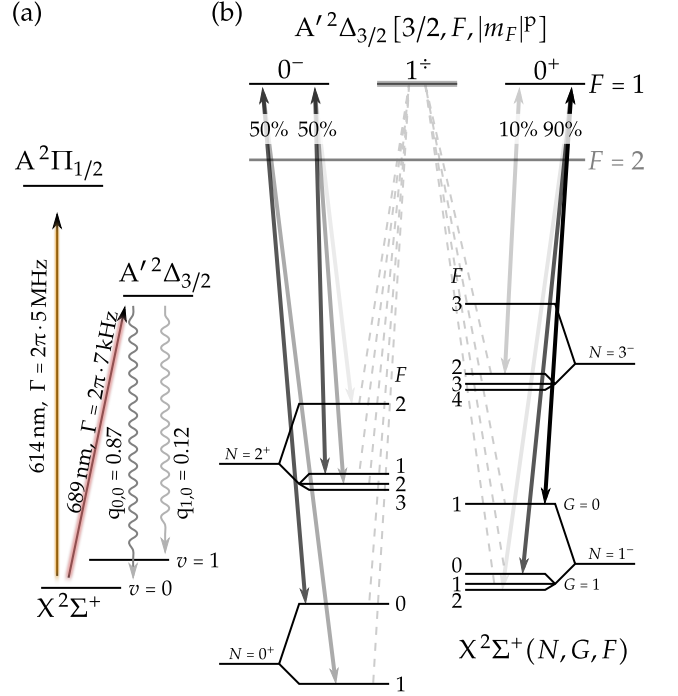


FIG. 2: (a) The relevant electronic states in YO with their transition wavelengths and radiative decay rates, along with the Franck-Condon factors $q_{v,v'}$ between the X and A' states for the first two vibrational states. (b) The allowed decay channels for the $A'{}^2\Delta_{3/2}[3/2, 1, |m_F|^P] \rightarrow X^2\Sigma^+$ transitions. The magnitude of each Clebsch-Gordan coefficient is represented by the relative brightness of the double-arrow to each ground state. Weak electric fields mixes the parity of $|m_F| = 1$ state, leading to a breakdown of the parity selection rule in dipole transitions.

approximate rotational closure, since decays to higher vibrational states (12%) are stronger than the loss to the $N = 3$ state. Therefore the ability to spectroscopically address the positive parity $A'{}^2\Delta_{3/2}[3/2, 1, 0^+]$ state is a necessity for quasi-closed cycling. This is achieved by utilizing the Stark effect and demonstrated in Sec. IV.

III. EXPERIMENTAL PROCEDURE AND STATE PREPARATION

All experiments in this study utilize an ultracold ensemble of ${}^{89}\text{Y}^{16}\text{O}$ molecules prepared in a single hyperfine sublevel of the lowest two rotational states of $X^2\Sigma^+$. The experimental apparatus and sequence are described throughout Refs. [36, 37], therefore we emphasize only key experimental details. A cold beam of YO with mean forward velocity of 160 m s^{-1} is produced by pulsed laser ablation of a ceramic Y_2O_3 target in a single-stage cryogenic helium buffer gas cell at 4 K. The molecules are decelerated by chirped laser slowing uti-

lizing the $A^2\Pi_{1/2} J = 1/2 \leftarrow X^2\Sigma^+ N = 1$ transitions. Sufficient cycling closure is achieved by additionally optically repumping the first two excited vibrational modes ($v = 1, 2$) of the $X^2\Sigma^+$ state. However, the $\Sigma - \Delta - \Pi$ electronic state configuration leads to weak violation of the rotational closure scheme. The low-lying $A'^2\Delta_{3/2}$ provides a two-photon decay pathway from $A^2\Pi_{1/2}$ to the even parity $X^2\Sigma^+ N = 0, 2$ electronic ground states. This leakage is resolved in the $v = 0$ manifold by mixing the $N = 1 \leftrightarrow N = 0$ ground states with resonant microwave radiation and optically pumping the $N = 2$ population into $N = 0$. With this scheme, molecules are slowed to $< 10 \text{ ms}^{-1}$ and captured by a dual frequency magneto-optical trap (MOT), routinely loading 10^5 molecules with a temperature of 2 mK. To further cool and compress the molecular cloud, a blue-detuned sub-Doppler MOT [37] is applied followed by a gray-molasses-cooling pulse providing number densities of approximately $1 \times 10^8 \text{ cm}^{-3}$ with a temperature of 3 μK .

Population transfer into a single quantum state $(N, G, F) = (1, 1, 0)$ is achieved by employing a near-resonant optical pumping sequence with two laser tones addressing the $A^2\Pi_{1/2} \leftarrow X^2\Sigma^+ (1, 1, \{1, 2\})$ and $(1, 0, 1)$ transitions [41]. This 500- μs long pulse transfers $\geq 95\%$ of the population into the target state at the expense of marginal heating to 4 μK . To mitigate further heating due to off-resonant scattering, the total intensity I of each laser tone is set to $s = I/I_{\text{sat}} \approx 0.05$. The saturation intensity is $I_{\text{sat}} = \pi\hbar c\Gamma/3\lambda^3$ where Γ and λ are the natural linewidth and transition wavelength, respectively. To initialize the molecules in an even-parity state, we transfer the $X^2\Sigma^+(1, 1, 0)$ population to the $X^2\Sigma^+(0, 1, 1)$ absolute ground state by applying an adiabatic Landau-Zener frequency-chirped microwave pulse. Following state preparation, all repump lasers and microwave tones are switched off unless otherwise stated.

After state preparation, a tunable electric field E_{appl} with field strength (0.25 to 0.75) V cm^{-1} is applied along the z direction opposing gravity. This weak field induces a Stark interaction between the near degenerate opposite-parity states in the $A'^2\Delta$ manifold. The field strength is chosen such that the interaction is strong compared to the Λ -doublet splitting ($\delta_{\Lambda}^{\Delta}$), but weak with respect to the hyperfine splitting between the $F = 1$ and $F = 2$ $A'^2\Delta_{3/2} J = 3/2$ excited states. This electric field tunability enables precision Stark spectroscopy of the $A'^2\Delta_{3/2} [J, F, |m_F|^{\text{p}}]$ states using a 689 nm external cavity diode laser. This narrow-linewidth laser is phase-locked to a low-noise erbium-doped fiber frequency comb, which is stabilized to an ultra stable monolithic cryogenic silicon cavity and referenced against the strontium clock transition [68, 69]. Circular-polarized spectroscopy light is coupled along the x - y MOT-laser-beam axes and can drive transitions with $\Delta m_F = 0, \pm 1$. After a 4-ms long interrogation time we measure the remaining population of the initialized state (Sec. IV) or the temperature of the molecular ensemble by time-of-flight expansion (Sec. V) as a function of the applied laser frequency.

IV. OPTICAL STARK SPECTROSCOPY

The long lifetime of the $A'^2\Delta$ state provides narrow transitions to the electronic ground state while the small Λ -doublet splitting leads to a large electric susceptibility. We investigated this by precision optical spectroscopy in the presence of a small applied electric field. The $A'^2\Delta_{3/2}[3/2, 1, |m_F|^{\text{p}}] \leftarrow X^2\Sigma^+$ transitions are resolved by measuring depletion signatures of the ground-state population following a 4-ms long exposure to the near-resonant laser. Molecules remaining within the initial ground state are measured by a fluorescent readout scheme utilizing the strong $A^2\Pi \leftarrow X^2\Sigma$ transition. Figure 3 (a) presents the normalized depletion ratio of the $(1, 1, 0)$ population as a function of detuning δ from the field-free transition frequency. The depletion was enhanced by employing the two-tone $N = 1$ optical pumping scheme via the broad transition to continuously repopulate the $(1, 1, 0)$ ground state during the laser interrogation sequence.

Each spectrum consists of three depletion dips corresponding to transitions to different field-dependent Stark states. The data is fit by three skewed Gaussians accounting for Doppler and inhomogeneous Stark broadening. Figure 3 (b) schematically illustrates the Stark interaction between the opposite-parity states of the Λ doublet. This field-dependent interaction is proportional to the magnitude of the magnetic quantum number $|m_F|$ and the effective electric dipole moment $\mu_{\text{eff}} \approx 3.8 \text{ D}$ (see Eq. (4) and Ref. [66], respectively). The resonant frequencies of the Stark-sensitive $|m_F| = 1$ states evolve linearly with the applied electric field strength [see Fig. 3 (a)]. This linear field dependence demonstrates full polarization of the $[3/2, 1, 1]$ states for each applied field. Comparing the field-insensitive central transition frequency against the center-of-gravity of the field-dependent transitions places an approximate upper bound $\delta_{\Lambda}^{\Delta} \leq 30 \text{ kHz}$. This experimentally constrained Λ -doublet splitting and the observed Stark shifts indicate the $A'^2\Delta_{3/2}$ state is fully polarized by field strengths $E_{\text{pol}} \approx 0.01 \text{ V cm}^{-1}$.

The unperturbed central depletion dip within each spectrum corresponds to the $m_F = 0$ transition frequency. This first-order Stark-insensitive state is used to define the field-free transition frequency and remains a pure parity eigenstate for all applied fields. Conversely, the field-dependent $|m_F| = 1$ states no longer possess definite parity when polarized. This explains their enhanced depletion within each spectrum, since parity-mixed states have access to additional decay pathways as shown in Fig. 2 (b) (dashed lines). A weak electric field of $\sim 0.5 \text{ V cm}^{-1}$ was applied throughout all following experiments. This field is sufficient to spectroscopically isolate the electric and magnetic field-insensitive $m_F = 0$ states within the center of the Stark manifold.

Figure 3 (c) presents ground state depletion measurements of both the $[3/2, 1, 0^+] \leftarrow (1, 1, 0)$ and the $[3/2, 1, 0^-] \leftarrow (0, 1, 1)$ transitions, with the corresponding frequen-

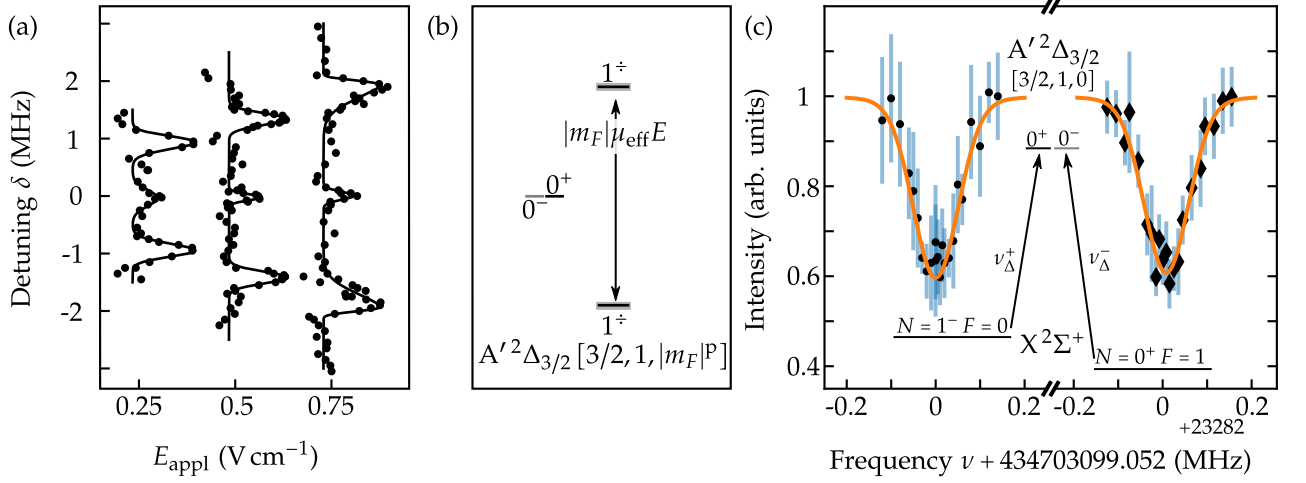


FIG. 3: Laser spectroscopy to the $A'^2\Delta_{3/2} [3/2, 1, |m_F|^P]$ states in the presence of a weak applied electric field E_{appl} . Panel (a) depicts the detuning-dependent depletion (solid dots) of the initial $(1, 1, 0)$ ground-state population for three different values of E_{appl} . Panel (b) shows the effect of the Stark interaction in the small field limit for the two field-sensitive and one field-insensitive state. Panel (c) presents spectra from the $(1, 1, 0)$ (solid dots) and $(0, 1, 1)$ (solid diamonds) ground states to the two opposite pure parity states of the $A'^2\Delta_{3/2} [3/2, 1, 0]$ state. A Gaussian lineshape model (orange lines) is used to obtain each center frequency.

cies denoted by ν_{Δ}^{+} and ν_{Δ}^{-} , respectively. The ground-state populations are initialized as discussed above in Sec. III. To prevent line distortions, only the spectroscopy laser with an intensity of $2I_{\text{sat}}$ was sent into the experimental chamber while all other sources of radiation were switched off. The normalized depletion signals from $N = 1$ (solid circles) and $N = 0$ (solid diamonds) are presented with their corresponding standard deviations (blue lines) derived from 60 measurements. The centroid transition frequencies were obtained from a weighted least-squares Gaussian lineshape fit, accounting for the dominant inhomogeneous Doppler broadening. To recover the absolute transition frequencies ν_{Δ}^{+} and ν_{Δ}^{-} the measurements were corrected by subtracting the recoil and quadratic Stark shifts. Table I summarizes the leading shifts and uncertainties considered for this absolute transition frequency determination.

TABLE I: Frequency corrections ($\delta\nu$) and uncertainties (σ) considered for determining the absolute transition frequencies ν_{Δ}^{+} and ν_{Δ}^{-} .

	$\delta\nu$ (kHz)	σ (kHz)
Recoil shift	3.99	0
Quadratic Stark shift	2.8	1.1
Doppler shift	0	0.08
Zeeman shift $(1, 1, 0)$	0	0
Zeeman shift $(0, 1, 1)$	0	1.5
Pressure shift	0	$\sim (10^{-6})$
BBR ac-Stark shift	0	0.1
ac-Stark shift	0	$\sim (10^{-2})$
Total	6.8	1.9

The quadratic Stark shift is calculated precisely using Eq. (3), the energy splitting to the nearest opposite-parity hyperfine state, and the observed first-order Stark shift of the field-sensitive states. The $A'^2\Delta_{3/2} J = 3/2$ $F = 2$ hyperfine state is measured to lie 105.3(3) MHz beneath the addressed $F = 1$ state. The uncertainty of the quadratic Stark shift is estimated from the inhomogeneous line broadening of the field-dependent states.

The first-order Doppler shift averages to zero by using a retroreflected, counter-propagating beam path. The associated uncertainty is derived assuming a maximal misalignment of 1 mrad between the counter-propagating beams and the velocity of the molecular cloud after 6 ms of free fall.

The $A'^2\Delta_{3/2} [3/2, 1, 0^{+}] \leftarrow X^2\Sigma^{+} (1, 1, 0)$ transition has no first order differential Zeeman shift and the earth magnetic field is actively compensated in all three dimensions to less than 5 mG. The transition involving the $X^2\Sigma^{+} (0, 1, 1)$ state is sensitive to a residual magnetic field and the Zeeman shift is estimated for a maximal population imbalance between the $m_F = \pm 1$ states of 10%.

The pressure shift, differential ac-Stark shift induced by black body radiation (BBR-shift), and ac-Stark shift induced by the spectroscopy laser are much smaller than the statistical uncertainty. The dominant contribution of the BBR-shift in the $A'^2\Delta_{3/2}$ arises from the $A^2\Pi_{3/2}$ state and is estimated to be ~ 10 Hz (following the procedure of Ref. [70]). The uncertainty for the BBR-shift is quoted to be 10 times this leading contribution, which is still well below our current experimental resolution. Close-lying hyperfine states are the leading contribution to ac-Stark shifts, which is calculated to be in the order of 10 Hz. The molecular density is too small for the van-

der-Waals interaction to perturb the observed transition frequency, even under the assumption of partial polarization.

Accounting for all considered shifts, the corrected transition frequencies of the $A'^2\Delta_{3/2}[3/2, 1, 0] \leftarrow X^2\Sigma^+$ transitions are:

$$\begin{aligned}\nu_{\Delta}^{+} &= 434\,680\,051\,302(3)_{\text{stat}}(1)_{\text{syst}}\text{kHz} \\ \nu_{\Delta}^{-} &= 434\,703\,333\,707(3)_{\text{stat}}(2)_{\text{syst}}\text{kHz}.\end{aligned}$$

These frequencies, with a relative uncertainty of 9×10^{-12} , comprise two of the most precise direct optical electronic transitions measured within a polar molecule. Additionally, the difference between the two obtained optical frequencies $\Delta\nu = \nu_{\Delta}^{-} - \nu_{\Delta}^{+} = 23\,282\,405(6)\text{kHz}$ is used to further constrain the $^2\Delta_{3/2}$ Λ -doublet splitting. Comparing $\Delta\nu$ against the well-known first rotational splitting of the $X^2\Sigma^+$ ground states $\nu_{(0,1,1)}^{(1,1,0)} = 23\,282\,405(4)\text{kHz}$ obtained by Fourier-transform microwave spectroscopy [71], reveals $\delta_{\Lambda}^{\Delta} = 0(7)\text{kHz}$. This result is in good agreement with the approximated value $\delta_{\Lambda}^{\Delta} \approx q\tau_{\Pi}/\tau_{\Delta} = 6\text{kHz}$ derived in Sec. II.

We demonstrated that a single quantum state of the $A'^2\Delta_{3/2}$ state with a well-defined parity can be excited in the presence of a weak electric field. This is crucial for laser cooling on the narrowline transition to constrain the decay pathways to a minimal set of ground states as discussed in Sec. II. Besides this, we used transitions between magnetic and electric field-insensitive states to measure optical transitions with an absolute accuracy 9×10^{-12} and constrained the Λ -doublet splitting to below 7 kHz by optical spectroscopy. Utilizing such transitions to the $A'^2\Delta_{5/2}$ state with its much longer lifetime is a potential candidate for an optical molecular lattice clock with unique physical properties attractive for testing fundamental physics, e.g., searching for a nuclear Schiff moment [72–75]. Alternatively, field-sensitive states of $A'^2\Delta_{5/2}$ are easily manipulated by weak electric fields. This provides a platform for dipole - dipole interactions with unprecedented interaction strength that can be engineered to realize strongly correlated many-body systems either in a bulk Bose gas or in a spin lattice [7].

V. NARROWLINE LASER COOLING

The pure parity $[3/2, 1, 0]$ excited states provide the optimal $A'^2\Delta_{3/2}$ cycling center for narrowline laser cooling. Although no strict rotational closure scheme exists for $^2\Delta \leftarrow ^2\Sigma^+$ transitions, the asymmetric branching from $[3/2, 1, 0^+]$ provides quasi-rotational closure within the $N = 1$ manifold [see Fig. 2 (b)]. Photon cycling via this single sublevel of the $A'^2\Delta_{3/2}$ excited state subsequently constrains the $X^2\Sigma^+$ ($1, G, F$) hyperfine sublevels amenable to laser cooling. Notably, $\Delta F = 0$ transitions between $m_F = 0$ sublevels are dipole forbidden, as well as $m'_F = 0 \leftarrow m_F = \pm 2$ transitions. Therefore, each hyperfine state within the $X^2\Sigma^+$ $N = 1$ manifold possess

dark sublevels except for the $(1,1,0)$ state. All subsequent data initializes the molecular population in this ground state as explained in Sec. III.

Narrowline laser cooling is demonstrated by employing the $A'^2\Delta[3/2, 1, 0^+] \leftarrow X^2\Sigma^+(1,1,0)$ transition. Cycling closure within the $N = 1$ manifold is achieved by continuously repopulating the $(1,1,0)$ state. Two additional laser tones optically repump the $(1,0,1)$ and $(1,1,\{1,2\})$ ground states via $A^2\Pi_{1/2}$. All rovibrational branching is optically pumped back to $N = 1$. This cooling scheme (right-hand side of Fig. 4 (a)) is applied for 4 ms while the molecular cloud is in free fall. The resulting radial temperatures (solid black squares) are obtained by time-of-flight measurements as a function of the static detuning δ from the narrowline transition resonance. The transition linewidth is power broadened with a saturation parameter $s = I/I_{\text{sat}} \approx 100$ to ensure the laser addresses broad classes of the molecular velocity distribution.

The radial temperature of the molecular ensemble rises to 10 μK due to off-resonant scattering from the $N = 1$ broadline repumpers. As the narrowline laser is scanned through resonance a strong temperature contrast is observed. The heating rate is damped when the laser is red detuned ($\delta < 0$) from the narrowline transition and enhanced when blue detuned ($\delta > 0$). The temperature evolution is modeled by the time-integrated solution to the one-dimensional momentum diffusion rate equation

$$\frac{1}{2}m\frac{d\langle v_x^2 \rangle}{dt} = \frac{d+3}{3}E_r R_{\text{scatt}} + \alpha \langle v_x^2 \rangle, \quad (5)$$

where m is the mass of $^{89}\text{Y}^{16}\text{O}$, $\langle v_x^2 \rangle$ the mean squared one-dimensional velocity, $d = 1,2,3$ is the dimensionality of laser cooling axes, E_r the photon recoil energy ($E_r/k_B = 384\text{nK}$), R_{scatt} the scattering rate, and α the damping coefficient. The scattering rate and damping coefficient incorporate the detuning dependence

$$R_{\text{scatt}} = \frac{\Gamma}{2} \frac{s}{1 + s + (2\delta/\Gamma)^2}, \quad (6)$$

$$\alpha = \frac{8\hbar k^2 s}{\Gamma} \frac{\delta}{[1 + s + (2\delta/\Gamma)^2]^2}, \quad (7)$$

where Γ is the natural linewidth of the narrow transition, and k is the corresponding wavenumber. The solution to the differential equation (5) provides a time evolution of $\langle v_x^2 \rangle$, corresponding to a radial temperature T according to $\langle v_x^2 \rangle = k_B T / 2m$. A least-squares optimized fit (black line) for this simple model agrees with the detuning-dependent temperature data, with the 95% confidence interval represented by the gray shaded region. The temperature evolution across the 300 kHz detuning range demonstrates the effect of narrowline Doppler cooling. Nevertheless, the photon scattering required to continuously optically pump the molecules to the $(1,1,0)$ ground state outpaces scattering on the narrowline transition.

Therefore any cycling scheme that implements repumping based on a broad transition provides cycling closure at the cost of heating.

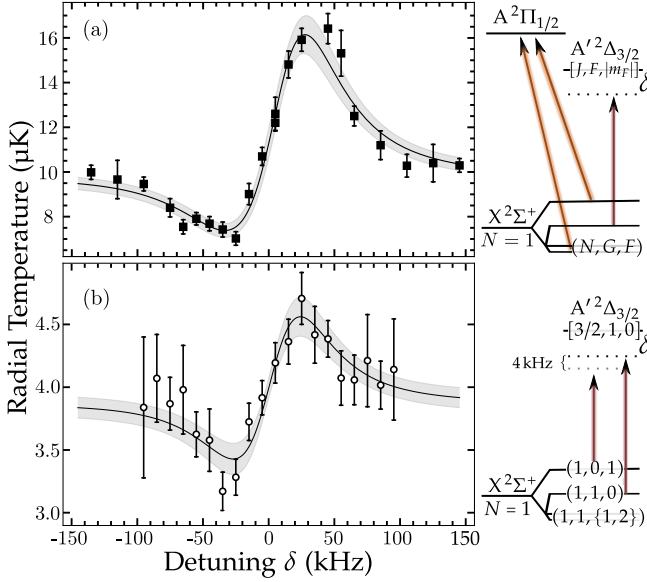


FIG. 4: Radial temperatures after employing a 4-ms long narrowline laser cooling sequence involving repump lasers connecting the $2\Pi_{1/2}$ state (a) and only narrowline transitions (b). A least-squares fit of a time-integrated momentum diffusion rate equation (black line) with the 95% confidence interval (gray shaded region) is used to model the detuning dependent cooling. The involved laser cooling schemes are depicted on the right-hand side.

To circumvent this heating, an alternative cooling scheme addressing only narrow transitions to the $A'^2\Delta_{3/2}$ state is implemented. The $[3/2, 1, 0^+]$ excited state predominately branches to two hyperfine levels within the $v = 0$ manifold: 33.33% to $(1,1,0)$ and 25% to each of the $(1,0,1)$ $|m_F| = 1$ degenerate sublevels. With all molecules initialized in the $(1,1,0)$ ground state, the two-tone narrowline laser cooling scheme (right-hand side of Fig. 4(b)) ensures no dark state population buildup and provides closure for 83.33% of the rotational branching pathways. Accounting for higher vibrational loss, the number of photons scattered is limited to $\langle n \rangle = 3.6$. This narrowline laser cooling scheme is applied for 4 ms while the molecular cloud is in free fall, with each tone power-broadened by a saturation parameter $s \approx 100$. The two tones are scanned in lockstep with a 4 kHz two photon detuning to prevent coherent effects. The resulting radial temperatures (open black circles) are presented as a function of δ from the $[3/2, 1, 0^+] \leftarrow (1,1,0)$ narrowline transition frequency in Fig. 4 (b).

Even with a limited photon budget ($\langle n \rangle = 3.6$), the temperature evolution recovers a Doppler cooling signature. Having eliminated the off-resonant repump heating, the initial 4 μ K radial temperature undergoes narrowline cooling (heating) as the laser is red (blue) detuned. The

temperature evolution is fit by Eq. 5 (black line) with the accompanying 95% confidence interval presented by the gray shaded region. The observed absolute temperature reduction of 800 nK to 3.2(2) μ K provides clear experimental evidence for the first narrowline laser cooling of molecules. The cooling effect is limited by the number of scattered photons and the 3.2 μ K radial temperature is approaching the Doppler temperature limit for the power-broadened transition linewidth. Both limitations can be overcome by cooling within a conservative trap.

The mean number of scattered photons can readily be enhanced by addressing all allowed decay pathways to the $v = 0$ ground state, namely the 10% branching to $(3,1,2)$ and 6.66% branching to $(1,1,2)$. The addition of two laser tones repumping these ground states via narrow transitions would double the number of photons scattered to $\langle n \rangle = 7.7$. Repumping the three $N = 1$ hyperfine states within the $v = 1$ manifold would enhance photon scattering to $\langle n \rangle = 45$. To implement these prospective cycling schemes the molecules would need to be loaded into an optical dipole trap to extend the laser interrogation time. AC Stark broadening from the trapping light could destabilize the narrowline cooling, however, this effect can be mitigated by applying a narrowline frequency sweep or employing a state-insensitive (magic) trap [76]. These conditions enable cooling to the photon recoil limit or to the motional ground state within a tightly confining optical lattice or tweezer.

VI. CONCLUSION

All current laser cooled molecules rely on rotationally closed cycling schemes exploiting a highly diagonal strong P(1) transition. While this recipe has enabled immense progress, the utility of other excited electronic states has largely remained unexplored. In particular, a subclass of molecules (MO) have a metastable $A'^2\Delta$ as their first excited state, which possesses near-degenerate opposite-parity sublevels and a long lifetime. How these novel features provide additional quantum control for molecules is demonstrated with ultracold YO throughout this study.

We first characterize the narrow transition through optical spectroscopy of the $A'^2\Delta_{3/2}$ Stark states. Spectroscopy taken across a series of applied electric fields reveal full polarization in the laboratory frame at $E_{\text{pol}} \approx 0.01 \text{ V cm}^{-1}$. Transition frequencies to opposite-parity field-insensitive states were measured with a relative uncertainty of 9×10^{-12} , constraining the $A'^2\Delta_{3/2}$ Λ -doublet splitting to $\delta_{\Lambda}^{\Delta} \leq 7 \text{ kHz}$. Pure parity excited states are isolated via the tunable Stark interaction and enable a quasi-closed photon cycling scheme.

Utilizing this electric field control, the first narrowline laser cooling of a molecule is achieved. The radial temperature of the molecular cloud was cooled by 0.8(2) μ K in free-space. Incorporating this cooling technique within an optical lattice is sufficient to initialize molecules in

their motional groundstate. This provides a pathway towards quantum simulation with directly laser-cooled molecules.

YO and all other MO molecules feature an even longer-lived $A'^2\Delta_{5/2}$ excited electronic state that is polarized by much smaller electric fields. Detailed spectroscopy is yet to be performed, however, this excited state is a prospective platform for electric field-induced collisional shielding, studies of strongly interacting dipolar physics,

and a molecular lattice clock.

Funding support for this work is provided by AFOSR MURI, ARO MURI, NIST, NSF QLCI OMA-2016244, and NSF PHY-2317149. We acknowledge A. Aeppeli, K. Kim, D. Lee, and B. Lewis for maintaining the optical reference frequency used in this work. We thank T. de Jongh and D. J. Nesbitt for careful reading of this manuscript.

-
- [1] J. P. Gordon, H. J. Zeiger, and C. H. Townes, Molecular Microwave Oscillator and New Hyperfine Structure in the Microwave Spectrum of NH_3 , *Physical Review* **95**, 282 (1954).
 - [2] J. J. Hudson, B. E. Sauer, M. R. Tarbutt, and E. A. Hinds, Measurement of the Electron Electric Dipole Moment Using YbF Molecules, *Physical Review Letters* **89**, 023003 (2002).
 - [3] V. Andreev, D. G. Ang, D. DeMille, J. M. Doyle, G. Gabrielse, J. Haefner, N. R. Hutzler, Z. Lasner, C. Meisenhelder, B. R. O'Leary, C. D. Panda, A. D. West, E. P. West, X. Wu, and ACME Collaboration, Improved limit on the electric dipole moment of the electron, *Nature* **562**, 355 (2018).
 - [4] T. S. Roussy, L. Caldwell, T. Wright, W. B. Cairncross, Y. Shagam, K. B. Ng, N. Schlossberger, S. Y. Park, A. Wang, J. Ye, and E. A. Cornell, An Improved Bound on the Electron's Electric Dipole Moment, *Science* **381**, 46 (2023).
 - [5] H. P. Büchler, E. Demler, M. Lukin, A. Micheli, N. Prokof'ev, G. Pupillo, and P. Zoller, Strongly Correlated 2D Quantum Phases with Cold Polar Molecules: Controlling the Shape of the Interaction Potential, *Physics Review Letters* **98**, 060404 (2007).
 - [6] K. Góral, L. Santos, and M. Lewenstein, Quantum Phases of Dipolar Bosons in Optical Lattices, *Physics Review Letters* **88**, 170406 (2002).
 - [7] T. Lahaye, C. Menotti, L. Santos, M. Lewenstein, and T. Pfau, The physics of dipolar bosonic quantum gases, *Reports on Progress in Physics* **72**, 126401 (2009).
 - [8] L. Pollet, J. D. Picon, H. P. Büchler, and M. Troyer, Supersolid Phase with Cold Polar Molecules on a Triangular Lattice, *Physics Review Letters* **104**, 125302 (2010).
 - [9] L. Christakis, J. S. Rosenberg, R. Raj, S. Chi, A. Morningstar, D. A. Huse, Z. Z. Yan, and W. S. Bakr, Probing site-resolved correlations in a spin system of ultracold molecules, *Nature* **614**, 64 (2023).
 - [10] C. Miller, A. N. Carroll, J. Lin, H. Hirzler, H. Gao, H. Zhou, M. D. Lukin, and J. Ye, Two-axis twisting using Floquet-engineered XYZ spin models with polar molecules, *Nature* **633**, 332 (2024).
 - [11] D. DeMille, Quantum Computation with Trapped Polar Molecules, *Physics Review Letters* **88**, 067901 (2002).
 - [12] S. F. Yelin, K. Kirby, and R. Côté, Schemes for robust quantum computation with polar molecules, *Physics Review A* **74**, 050301 (2006).
 - [13] M. Karra, K. Sharma, B. Friedrich, S. Kais, and D. Herschbach, Prospects for quantum computing with an array of ultracold polar paramagnetic molecules, *The Journal of Chemical Physics* **144**, 10.1063/1.4942928 (2016).
 - [14] S. L. Cornish, M. R. Tarbutt, and K. R. A. Hazzard, Quantum computation and quantum simulation with ultracold molecules, *Nature Physics* **20**, 730 (2024).
 - [15] C. Zhang and M. Tarbutt, Quantum computation in a hybrid array of molecules and rydberg atoms, *PRX Quantum* **3**, 030340 (2022).
 - [16] K.-K. Ni, S. Ospelkaus, D. Wang, G. Quémener, B. Neyenhuis, M. H. G. de Miranda, J. L. Bohn, J. Ye, and D. S. Jin, Dipolar collisions of polar molecules in the quantum regime, *Nature* **464**, 1324 (2010).
 - [17] R. Bause, A. Christianen, A. Schindewolf, I. Bloch, and X.-Y. Luo, Ultracold Sticky Collisions: Theoretical and Experimental Status, *The Journal of Physical Chemistry A* **127**, 729 (2023).
 - [18] I. I. Rabi, S. Millman, P. Kusch, and J. R. Zacharias, The Molecular Beam Resonance Method for Measuring Nuclear Magnetic Moments. The Magnetic Moments of ${}^3\text{Li}^6$, ${}^3\text{Li}^7$ and ${}^9\text{F}^{19}$, *Physics Review* **55**, 526 (1939).
 - [19] S. Y. T. van de Meerakker, H. L. Bethlem, and G. Meijer, Taming molecular beams, *Nature Physics* **4**, 595 (2008).
 - [20] D. Reens, H. Wu, A. Aepli, A. McAuliffe, P. Wcisło, T. Langen, and J. Ye, Beyond the limits of conventional stark deceleration, *Physics Review Research* **2**, 033095 (2020).
 - [21] P. Jansen and F. Merkt, Manipulating beams of paramagnetic atoms and molecules using inhomogeneous magnetic fields, *Progress in Nuclear Magnetic Resonance Spectroscopy* **120–121**, 118 (2020).
 - [22] R. E. Drullinger and R. N. Zare, Optical Pumping of Molecules, *The Journal of Chemical Physics* **51**, 5532 (1969).
 - [23] X. Wu, Z. Han, J. Chow, D. G. Ang, C. Meisenhelder, C. D. Panda, E. P. West, G. Gabrielse, J. M. Doyle, and D. DeMille, The metastable $Q^3\Delta_2$ state of ThO: a new resource for the ACME electron EDM search, *New Journal of Physics* **22**, 023013 (2020).
 - [24] M. D. Rosa, Laser-cooling molecules: Concept, candidates, and supporting hyperfine-resolved measurements of rotational lines in the A-X(0,0) band of CaH, *The European Physical Journal D* **31**, 395 (2004).
 - [25] B. K. Stuhl, B. C. Sawyer, D. Wang, and J. Ye, Magneto-optical trap for polar molecules, *Physical Review Letters* **101**, 243002 (2008).
 - [26] V. Zhelyazkova, A. Cournol, T. E. Wall, A. Matsushima, J. J. Hudson, E. Hinds, M. Tarbutt, and B. Sauer, Laser cooling and slowing of CaF molecules, *Physical Review A* **89**, 053416 (2014).
 - [27] M. T. Hummon, M. Yeo, B. K. Stuhl, A. L. Collopy, Y. Xia, and J. Ye, 2D Magneto-Optical Trapping of Diatomic Molecules, *Physics Review Letters* **110**, 143001

- (2013).
- [28] B. Hemmerling, E. Chae, A. Ravi, L. Anderegg, G. K. Drayna, N. R. Hutzler, A. L. Collopy, J. Ye, W. Ketterle, and J. M. Doyle, Laser slowing of CaF molecules to near the capture velocity of a molecular MOT, *Journal of Physics B: Atomic, Molecular and Optical Physics* **49**, 174001 (2016).
 - [29] J. F. Barry, D. J. McCarron, E. B. Norrgard, M. H. Steinecker, and D. DeMille, Magneto-optical trapping of a diatomic molecule, *Nature* **512**, 286 (2014).
 - [30] M. R. Tarbutt and T. C. Steimle, Modeling magneto-optical trapping of CaF molecules, *Physics Review A* **92**, 053401 (2015).
 - [31] L. Anderegg, B. L. Augenbraun, E. Chae, B. Hemmerling, N. R. Hutzler, A. Ravi, A. Collopy, J. Ye, W. Ketterle, and J. M. Doyle, Radio Frequency Magneto-Optical Trapping of CaF with High Density, *Physics Review Letters* **119**, 103201 (2017).
 - [32] A. L. Collopy, S. Ding, Y. Wu, I. A. Finneran, L. Anderegg, B. L. Augenbraun, J. M. Doyle, and J. Ye, 3D Magneto-Optical Trap of Yttrium Monoxide, *Physics Review Letters* **121**, 213201 (2018).
 - [33] Z. Zeng, S. Deng, S. Yang, and B. Yan, Three-Dimensional Magneto-Optical Trapping of Barium Monofluoride, *Physics Review Letters* **133**, 143404 (2024).
 - [34] S. Truppe, H. Williams, M. Hambach, L. Caldwell, N. Fitch, E. Hinds, B. Sauer, and M. Tarbutt, Molecules cooled below the Doppler limit, *Nature Physics* **13**, 1173 (2017).
 - [35] K. N. Jarvis, J. A. Devlin, T. E. Wall, B. E. Sauer, and M. R. Tarbutt, Blue-detuned magneto-optical trap, *Physics Review Letters* **120**, 083201 (2018).
 - [36] S. Ding, Y. Wu, I. A. Finneran, J. J. Burau, and J. Ye, Sub-Doppler cooling and compressed trapping of YO molecules at μK temperatures, *Physical Review X* **10**, 021049 (2020).
 - [37] J. J. Burau, P. Aggarwal, K. Mehling, and J. Ye, Blue-Detuned Magneto-optical Trap of Molecules, *Physical Review Letters* **130**, 193401 (2023).
 - [38] C. Hallas, G. K. Li, N. B. Vilas, P. Robichaud, L. Anderegg, and J. M. Doyle, High Compression Blue-Detuned Magneto-Optical Trap of Polyatomic Molecules (2024).
 - [39] S. S. Yu, J. You, Y. Bao, L. Anderegg, C. Hallas, G. K. Li, D. Lim, E. Chae, W. Ketterle, K.-K. Ni, and J. M. Doyle, A conveyor-belt magneto-optical trap of CaF (2024).
 - [40] V. Jorapur, T. K. Langin, Q. Wang, G. Zheng, and D. DeMille, High Density Loading and Collisional Loss of Laser-Cooled Molecules in an Optical Trap, *Physics Review Letters* **132**, 163403 (2024).
 - [41] J. J. Burau, K. Mehling, M. D. Frye, M. Chen, P. Aggarwal, J. M. Hutson, and J. Ye, Collisions of spin-polarized YO molecules for single partial waves, *Physics Review A* **110**, L041306 (2024).
 - [42] M. Yeo, M. T. Hummon, A. L. Collopy, B. Yan, B. Hemmerling, E. Chae, J. M. Doyle, and J. Ye, Rotational State Microwave Mixing for Laser Cooling of Complex Diatomic molecules, *Phys. Rev. Lett.* **114**, 223003 (2015).
 - [43] A. L. Collopy, M. T. Hummon, M. Yeo, B. Yan, and J. Ye, Prospects for a narrow line MOT in YO, *New Journal of Physics* **17**, 055008 (2015).
 - [44] S. Truppe, S. Marx, S. Kray, M. Doppelbauer, S. Hofsäss, H. C. Schewe, N. Walter, J. Pérez-Ríos, B. G. Sartakov, and G. Meijer, Spectroscopic characterization of aluminum monofluoride with relevance to laser cooling and trapping, *Physics Review A* **100**, 052513 (2019).
 - [45] J. Kobayashi, K. Aikawa, K. Oasa, and S. Inouye, Prospects for narrow-line cooling of KRb molecules in the rovibrational ground state, *Physics Review A* **89**, 021401 (2014).
 - [46] S. Yi, T. Li, and C. P. Sun, Novel quantum phases of dipolar bose gases in optical lattices, *Physics Review Letters* **98**, 260405 (2007).
 - [47] K. Matsuda, L. De Marco, J.-R. Li, W. G. Tobias, G. Valtolina, G. Quémener, and J. Ye, Resonant collisional shielding of reactive molecules using electric fields, *Science* **370**, 1324 (2020).
 - [48] G. Quémener and J. L. Bohn, Shielding $^2\Sigma$ ultracold dipolar molecular collisions with electric fields, *Physics Review A* **93**, 012704 (2016).
 - [49] M. Schmidt, L. Lassablière, G. Quémener, and T. Langen, Self-bound Dipolar Droplets and Supersolids in Molecular Bose-Einstein Condensates, *Physics Review Research* **4**, 013235 (2022).
 - [50] R. Stringat, C. Athénour, and J. L. Féménias, Analyse Rotationnelle de la Bande (0,0) du Système Orange de ScO, *Canadian Journal of Physics* **50**, 395 (1972).
 - [51] W. J. Childs and T. C. Steimle, A molecular-beam-optical and radio frequency-optical double-resonance study of the $A^2\Pi-X^2\Sigma^+$ band system of scandium monoxide, *The Journal of Chemical Physics* **88**, 6168 (1988).
 - [52] Q.-S. Yang, Y.-F. Gao, Y. Yu, and T. Gao, Ab initio study of the feasibility of laser cooling of ScO molecule, *Molecular Physics* **114**, 870 (2016).
 - [53] A. Bernard and A. M. Sibai, The Spectrum of Lanthanum Oxide: A Reanalysis of the Rotational Data, *Zeitschrift für Naturforschung A* **35**, 1313 (1980).
 - [54] C. Zhang, H. Korslund, Y. Wu, S. Ding, and L. Cheng, Towards accurate prediction for laser-coolable molecules: relativistic coupled-cluster calculations for yttrium monoxide and prospects for improving its laser cooling efficiencies, *Physical Chemistry Chemical Physics* **22**, 26167 (2020).
 - [55] A. Bernard, R. Bacis, and P. Luc, Fourier Transform Spectroscopy: Extensive Analysis of the $A^2\Pi-X^2\Sigma^+$ and $B^2\Sigma^+-X^2\Sigma^+$ Systems of Yttrium Oxide, *The Astrophysical Journal* **227**, 338 (1979).
 - [56] R. Suenram, F. Lovas, G. Fraser, and K. Matsumura, Pulsed-nozzle Fourier-transform microwave spectroscopy of laser-vaporized metal oxides: Rotational spectra and electric dipole moments of YO, LaO, ZrO, and HfO, *The Journal of chemical physics* **92**, 4724 (1990).
 - [57] P. F. Bernath, R. Dodangodage, and J. Liévin, S-type Stars: LaO Line List for the $B^2\Sigma^+-X^2\Sigma^+$ Band System, *The Astrophysical Journal* **933**, 99 (2022).
 - [58] P. F. Bernath, R. Dodangodage, and J. Liévin, S-type Stars: Line List for the $A^2\Pi-X^2\Sigma^+$ Band System of LaO, *The Astrophysical Journal* **953**, 181 (2023).
 - [59] C. L. Chalek and J. L. Gole, Chemiluminescence spectra of ScO and YO: Observation and analysis of the $A'^2-X^2\Sigma^+$ band system, *The Journal of Chemical Physics* **65**, 2845 (1976).
 - [60] J. M. Brown and A. Carrington, *Rotational Spectroscopy of Diatomic Molecules*, Cambridge Molecular Science (Cambridge University Press, 2003).
 - [61] J. K. Watson, Hönl-London factors for multiplet transi-

- tions in Hund's case a or b, *Journal of Molecular Spectroscopy* **252**, 5 (2008).
- [62] J. H. Van Vleck, On σ -Type Doubling and Electron Spin in the Spectra of Diatomic Molecules, *Physical Review* **33**, 467 (1929).
 - [63] R. S. Mulliken and A. Christy, Λ -Type Doubling and Electron Configurations in Diatomic Molecules, *Physical Review* **38**, 87 (1931).
 - [64] H. Lefebvre-Brion and R. W. Field, *The Spectra and Dynamics of Diatomic Molecules* (Elsevier, Amsterdam, 2004).
 - [65] J. M. Brown, A. S.-C. Cheung, and A. J. Merer, Λ -Type doubling parameters for molecules in Δ electronic states, *Journal of Molecular Spectroscopy* **124**, 464 (1987).
 - [66] A. N. Smirnov, V. G. Solomonik, S. N. Yurchenko, and J. Tennyson, Spectroscopy of YO from first principles, *Physical Chemistry Chemical Physics* **21**, 22794 (2019).
 - [67] J. M. Brown and B. J. Howard, An approach to the anomalous commutation relations of rotational angular momenta in molecules, *Molecular Physics* **31**, 1517 (1976).
 - [68] E. Oelker, R. B. Hutson, C. J. Kennedy, L. Sonderhouse, T. Bothwell, A. Goban, D. Kedar, C. Sanner, J. M. Robinson, G. E. Marti, D. G. Matei, T. Legero, M. Giunta, R. Holzwarth, F. Riehle, U. Sterr, and J. Ye, Demonstration of 4.8×10^{-17} stability at 1 s for two independent optical clocks, *Nature Photonics* **13**, 714 (2019).
 - [69] A. Aepli, K. Kim, W. Warfield, M. S. Safronova, and J. Ye, Clock with 8×10^{-19} systematic uncertainty, *Physics Review Letters* **133**, 023401 (2024).
 - [70] J. W. Farley and W. H. Wing, Accurate calculation of dynamic Stark shifts and depopulation rates of Rydberg energy levels induced by blackbody radiation. Hydrogen, helium, and alkali-metal atoms, *Physical Review A* **23**, 2397 (1981).
 - [71] R. D. Suenram, F. J. Lovas, G. T. Fraser, and K. Matsumura, Pulsed-nozzle Fourier-transform microwave spectroscopy of laser-vaporized metal oxides: Rotational spectra and electric dipole moments of YO, LaO, ZrO, and HfO, *The Journal of Chemical Physics* **92**, 4724 (1990).
 - [72] M. G. Kozlov and L. N. Labzowsky, Parity violation effects in diatomics, *Journal of Physics B: Atomic, Molecular and Optical Physics* **28**, 1933 (1995).
 - [73] V. Spevak, N. Auerbach, and V. V. Flambaum, Enhanced t -odd, p -odd electromagnetic moments in reflection asymmetric nuclei, *Phys. Rev. C* **56**, 1357 (1997).
 - [74] V. V. Flambaum and H. Feldmeier, Enhanced nuclear Schiff moment in stable and metastable nuclei, *Phys. Rev. C* **101**, 015502 (2020).
 - [75] V. V. Flambaum, V. A. Dzuba, and H. B. T. Tan, Time- and parity-violating effects of the nuclear Schiff moment in molecules and solids, *Phys. Rev. A* **101**, 042501 (2020).
 - [76] K. Leung, I. Majewska, H. Bekker, C.-H. Lee, E. Tiberi, S. Kondov, R. Moszynski, and T. Zelevinsky, Transition strength measurements to guide magic wavelength selection in optically trapped molecules, *Physical Review Letters* **125**, 153001 (2020).